Received March 6, 2021, accepted March 21, 2021, date of publication March 29, 2021, date of current version April 9, 2021.

Digital Object Identifier 10.1109/ACCESS.2021.3069185

A Metasurface-Based MIMO Antenna for 5G Millimeter-Wave Applications

SABA TARIQ[1], SYEDA I. NAQVI[1], NIAMAT HUSSAIN[2], (Member, IEEE), AND YASAR AMIN[1], (Senior Member, IEEE)

[1]Department of Telecommunication Engineering, University of Engineering and Technology, Taxila 47050, Pakistan
[2]Department of Computer and Communication Engineering, Chungbuk National University, Cheongju 28644, South Korea

Corresponding authors: Syeda I. Naqvi (iffat.naqvi@uettaxila.edu.pk) and Niamat Hussain (hussain@chungbuk.ac.kr)

ABSTRACT This work presents a 4-element multiple-input multiple-output (MIMO) antenna with a single layered metasurface array for fifth generation (5G) millimeter-Wave (mm-Wave) communication systems. Each MIMO antenna element is composed of a 1 × 2 array with a corporate feed network. Moreover, a metasurface array structure consisting of 9 × 6 Circular Split Ring (CSR) shaped cells is employed to improve the gain and isolation between the MIMO antenna elements. The proposed antenna system is realized using 0.787 mm thick Rogers RT Duroid 5880 substrate. The performance of the antenna is investigated in terms of s-parameters, radiation characteristics, and MIMO parameters. The antenna operates at the mm-Wave frequency band ranging from 24.55 to 26.5 GHz. The incorporation of the metasurface layer enhanced the gain thus attaining a peak measured gain of 10.27 dBi. Additionally, isolation is also improved by 5dB after the employment of metasurface. The investigation of MIMO performance metrics such as Envelope Correlation Coefficient (ECC), Diversity Gain (DG), Channel Capacity Loss (CCL), and Mean Effective Gain (MEG) exhibits good antenna characteristics. The demonstrated radiation properties of the proposed antenna ascertain its suitability for the forthcoming 5G communication systems.

INDEX TERMS Antenna array, 5G, millimeter-wave, MIMO antenna, metamaterial.

I. INTRODUCTION

Due to a tremendous increase in the annual data traffic (40% to 70%), wireless networks may require 1000 times more capacity in the coming years as compared to the current requirement. In order to meet this exponentially growing demand, the fifth generation (5G) systems with the peak throughput of multi gigabits per second (Gb/s) are considered to be the substantial solution for future communication applications [1]–[3]. The limited channel capacity and restricted bandwidth at the sub-6 GHz band have impelled academic researchers and engineers to use the underutilized mm-Wave spectrum for 5G wireless communication systems [4], [5]. This impending 5G technology is not only crucial to fulfilling the immensely growing data rates demands, low power consumption, and reliability for massively increasing number of connected devices, but also reinforces the capabilities of the incipient technologies like smart cities, Internet of Vehicles, and virtual reality [6]. Conversely, the signal degradation factors such as atmospheric absorptions and path loss attenuation increase at the mm-Wave Spectrum [5]. As the frequency band allocation is of prime significance in the modeling of any communication system; therefore the world's telecom industry and regulatory bodies are doing tremendous work in the regularization of the 5G communication networks. A brief overview of the region wise mm-Wave spectrum allocation for 5G is shown in Figure 1. It is depicted that most of the countries are considering 26/28 GHz band for 5G communication [1], [7]. Also, antennas are the primary constituents for the successful deployment of communication networks. Therefore, the antenna design is of great significance to realize communication at the mmWave frequencies. These 5G systems are expected to have numerous antennas at the base station and also at user terminals. Also, the arrays, MIMO, and beamforming technologies are considered to be the key enablers for 5G mm-Wave communication [4]. Recently, numerous research works have explored antenna designs for the potential mm-Wave bands [8]–[40]. In order to address the higher attenuation at mm-Wave spectrum, high gain antenna arrays with beam steering capability have been investigated extensively offering increased signal strength and significant spatial coverage [8]–[17]. Although the antenna gain

The associate editor coordinating the review of this manuscript and approving it for publication was Mohsen Khalily.

	< 1 GHz	3 GHz	4 GHz	5 GHz	24-28 GHz	37-40 GHz	64-71 GHz
	600 MHz	3.5 GHz		5.9-7.1 GHz	27.5-28.35 GHz	37-37.6 GHz	64-71 GHz
	600 MHz	3.5 GHz		5.9-7.1 GHz	27.5-28.35 GHz	37-40 GHz	64-71 GHz
	700 MHz	3.4-3.8 GHz		5.9-6.4 GHz	24.5-27.5 GHz	37-37.6 GHz	
		3.4-3.8 GHz			26, 28 GHz	37-40 GHz	
		3.4-3.7 GHz			26, 28 GHz		
		3.46-3.8 GHz			26 GHz		
		3.6-3.8 GHz					
		3.3-3.6 GHz			24.5-27.5 GHz	37-42.5 GHz	
		3.4-3.7 GHz	4.8-5 GHz		26.5-29.5 GHz		
		3.6-4.2 GHz			27.5-29.5 GHz		
		3.4-3.7 GHz	4.4-4.9 GHz		28 GHz	39 GHz	

FIGURE 1. Overview of the global spectrum allocation for 5G.

increases with the increasing number of radiators in an array, however larger array structures have inevitable losses across the power divider. Therefore, high gain antennas with a low profile are of substantial importance. Various antenna designs have been investigated to increase the gain maintaining a low profile. This includes metamaterial-based antennas, lens-coupled antennas, and Fabry-Perot cavity antennas [18]–[25]. Moreover, despite the attainment of high gain (necessary to mitigate the effects of increased attenuation and atmospheric absorptions), these antennas exhibit the same capacity as a single element due to a single feed port. To enhance the communication system capacity, MIMO technology is considered to be of great significance as it enables the multiple antennas to operate concurrently, thus improving the data rate, capacity, and reliability of the communication link. Several literary works reported MIMO antennas operating at mm-wave frequency band [26]–[32]. The antennas presented in these works demonstrate good MIMO performance with significant isolation. However, the gain exhibited by these MIMO antennas is comparatively low.

In recent years, metamaterials have been investigated extensively owing to their various electromagnetic characteristics not commonly present in natural materials [33]. Several works reported mm-wave MIMO antennas with metamaterial structures to enhance the antenna performance, particularly reduction in mutual coupling or antenna gain improvement [34]–[40]. The work in [34] proposed a 2 × 2 mm-wave MIMO antenna with bi-layered Frequency Selective Surface (FSS) superstrate for addressing the mutual coupling effects. Due to the FSS integration, a 6-12 dB improvement in isolation is obtained for the proposed MIMO antennas. Similarly, in [35] another technique is presented to decrease the coupling amid the MIMO antennas. In this work, metamaterial based corrugations are etched on the long edges of the substrate. As a result, enhancement of 12-15 dB isolation is observed. The presented antenna also obtains high gain. However, the substrate size of the proposed design is 21 mm × 85 mm, which is relatively large. In [36], a metamaterial based polarization-rotator (PR) wall is integrated to enhance isolation amid mm-wave DRAs. On average, 16 dB reduction in mutual coupling is attained by using this technique. The design proposed in [37] demonstrated an Electromagnetic band-gap (EBG) reflector positioned below the two-port MIMO antenna to enhance the antenna gain. The peak gain obtained for the proposed geometry is 11.5 dBi. Although the antenna exhibited good MIMO performance and high gain, however, the presented overall structure possesses comparatively large dimensions, which limit its suitability for the future miniaturized communication devices. Moreover, the bow-tie shaped mm-wave MIMO antenna in [38] is integrated with three pairs of metamaterial arrays to enhance gain. The maximum gain obtained by this antenna is 7.4 dBi. In [39], a two-port mm-wave MIMO antenna is reported with EBG structure for gain improvement. The introduction of EBG enhances gain by 1.9 dBi with a peak gain of 6 dBi. In [40], a DRA with four element MIMO configuration is proposed for mm-Wave applications. A metamaterial structure is printed on the top side of the DRA to enhance isolation. Due to the involvement of metamaterial, a 12-13 dB increase is observed in isolation between the MIMO elements. The maximum gain achieved for the operational frequency band is 7 dBi which is relatively low. This discussion reveals that these research studies either focus on gain enhancement or isolation improvement. However, both of these factors are important for the antenna to perform efficiently.

Considering the limitations as experienced by the antenna designs discussed above, this work proposed a four-element MIMO antenna for mm-wave 5G communication devices involving metasurface for gain and isolation enhancement. In order to enhance gain, a single element antenna is modified to array structure. Thus, each MIMO antenna comprises of 1 × 2 element array fed with a parallel feeding network. To further enhance gain and to decrease the coupling effects between the MIMO elements, a metasurface of periodically patterned 9 × 6 Circular Split Ring (CSR) shaped cells is placed above the MIMO antennas. The final proposed antenna covers the mm-Wave frequency band 24.55-26.5 GHz supporting 5G applications. A prominent increase in gain is observed with a peak gain value of 10.27 dBi. In addition, an improvement in isolation is attained after the introduction of the metasurface.

II. ANTENNA GEOMETRY AND DESIGN PROCEDURE

The proposed antenna design consists of a 4-element MIMO antenna structure with a substrate size of 30 mm × 43 mm. The substrate used is Rogers RT/Duroid 5880 with $\varepsilon_r = 2.2$ and thickness of h = 0.787 mm. In addition, a metasurface array of periodically arranged 9 × 6 Circular Split Ring (CSR) shaped unit cells is placed above the MIMO antennas at the height of approximately 0.42 λ to optimize

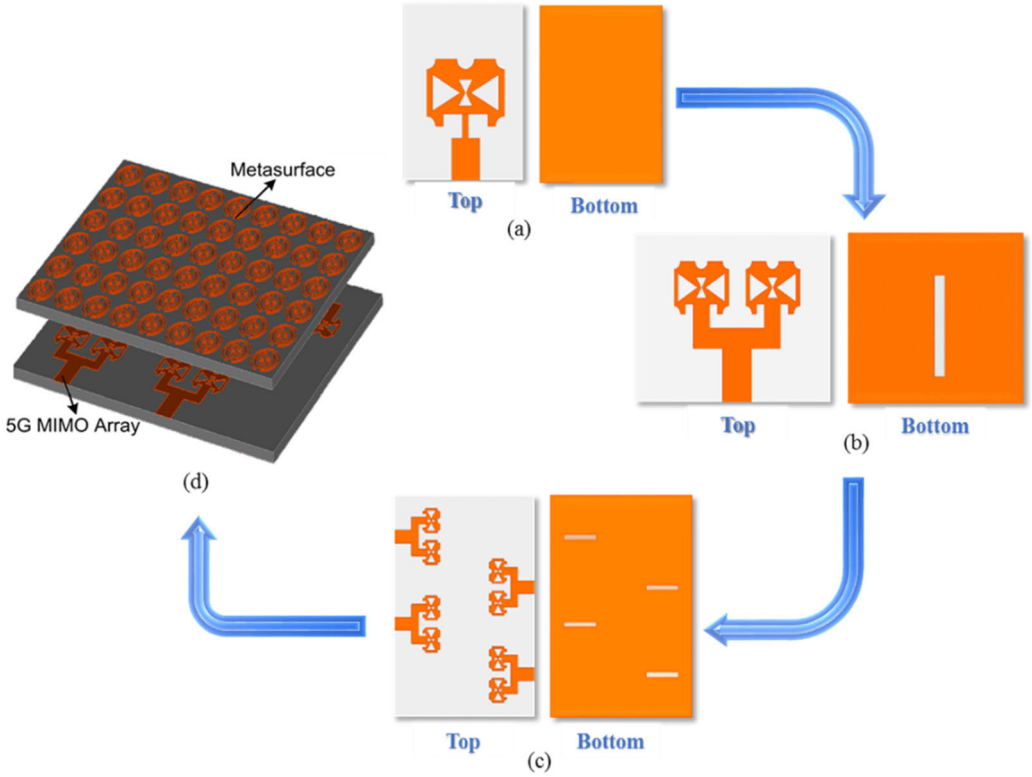

FIGURE 2. Stepwise design progression (a) Single antenna (b) 1 × 2 element array (c) MIMO antenna system (d) MIMO antenna with metasurface.

the antenna performance. The commercially available EM simulator CST Microwave Studio is used for the modeling and simulation of this design. Figure. 2 illustrates an overview of the stepwise design progression. The subsequent sections provide a detailed discussion on the stepwise design procedure, the optimization techniques employed, and relevant obtained results.

A. ANTENNA DESIGN

The modeling of the design starts from a single antenna element, as illustrated in Figure. 3 (a). In the first step, a rectangular patch antenna with inset feed and the full ground plane is obtained using well established mathematical equations [41], resonating for the 26 GHz frequency band with 0.9 GHz bandwidth, as shown in Figure. 3 (b). In the second step, the rectangular patch antenna is optimized by etching bow-tie shaped slots both vertically and horizontally. This optimization improves the impedance matching [42], [43], and a bandwidth of 1.18 GHz is obtained with a resonant band of 23.9-25.08 GHz. The third and final optimization step involves the etching of semicircular slots at the four corners and at the top side of the antenna. This antenna covers a band from 25-26.2 GHz with 1.2 GHz impedance bandwidth, as illustrated by the reflection coefficient curve in Figure. 3 (b). Although shifting of bands has been observed for three optimization steps due to change in electrical length of the antenna, however, the overall impedance bandwidth has improved. The optimized dimensions of the final single antenna are provided in Table 1.

In order to improve the radiation characteristics, the single antenna is modified to an array with two elements fed by a parallel feed line, as shown in Figure. 4 (a). The widths of the transmission lines are calculated using the characteristic equations given as (1-7) to match the impedance of the main feed line at 50 Ω, whereas of the branched network at 100Ω [41].

For $\frac{W_a}{h} \leq 1$

$$Z_o = \frac{60}{\varepsilon_{reff}} \ln\left(\frac{8h}{W_a} + \frac{W_a}{4h}\right) \tag{1}$$

where,

$$\varepsilon_{reff} = \frac{\varepsilon_r + 1}{2} + \frac{\varepsilon_r - 1}{2}\left(\frac{1}{\sqrt{1 + 12\frac{h}{W_a}}} + 0.004\left(1 - \frac{W_a}{h}\right)^2\right) \tag{2}$$

For $\frac{W_a}{h} \geq 1$

$$Z_o = \frac{120\pi\sqrt{\varepsilon_{reff}}}{\frac{W_a}{h} + 1.393 + 0.667\ln\left(\frac{W_a}{h} + 1.444\right)} \tag{3}$$

where,

$$\varepsilon_{reff} = \frac{\varepsilon_r + 1}{2} + \frac{\varepsilon_r - 1}{2}$$

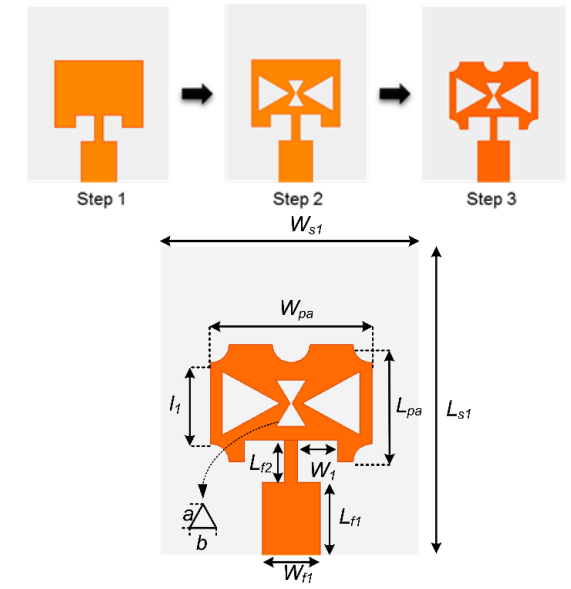

(a)

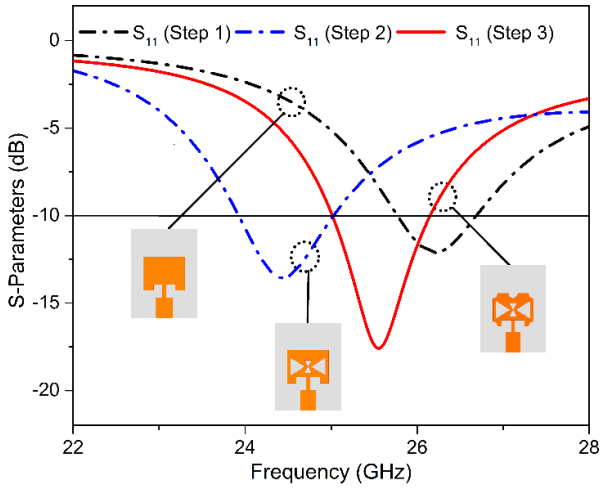

(b)

FIGURE 3. (a) Single element design evolution (b) S-parameter curves.

$$\times \left(\frac{1}{\sqrt{1+12\frac{h}{W_a}}} + 0.004\left(1-12\frac{h}{W_a}\right)^{-\frac{1}{2}} \right) \quad (4)$$

where Z_0 represents the characteristic impedance of the transmission line, W_a is the width of the feedline. ε_r is the dielectric constant and ε_{reff} is the effective permittivity. The length and width of the feed network are calculated by using the equations given below.

$$W_a = \frac{2h}{\pi}\left(B - 1 + \frac{\varepsilon_r - 1}{2\varepsilon_r}\left[\ln(B-1) + 0.39 - \frac{0.61}{\varepsilon_r}\right]\right) \quad (5)$$

$$L_a = \frac{\lambda}{4\sqrt{\varepsilon_{reff}}} \quad (6)$$

$$B = \frac{60\pi^2}{Z_o\sqrt{\varepsilon_r}} \quad (7)$$

TABLE 1. Optimized parameters of proposed design (in millimeter).

Par.	Value	Par.	Value	Par.	Value
		Single element Parameters			
W_{s1}	7.7	W_{pa}	4.7	W_{f1}	1.7
L_{s1}	9.5	L_{pa}	3.5	L_{f1}	2.2
a	0.2	b	0.2	L_{f2}	1.2
l_1	2.4				
		Two element Array Parameters			
W_{s2}	17	W_a	2.5	W_c	1
L_{s2}	11.7	L_a	3.7	L_c	*6.8*
p_a	1.4	L_{cd}	3		
		Unit Cell of Metamaterial			
W_u	5	g_1	0.7	g_3	0.4
L_u	5	g_2	0.7		
		Metasurface Parameters			
W_m	*28*	L_m	*41*	g	1
h_t	*0.5λ*				

Here, B is basically a constant used in the inverse design formula given in (5) for a microstrip line of the given characteristic impedance, and L_a is the length of the feedline. The gap p_a amid the two elements of an array is 1.437mm, nearly equal to 0.125λ at 26 GHz, which demonstrates the compactness of the design. Moreover, a vertical slot of length L_c and width W_c is incorporated at the ground plane. This design optimization from a single element to array enables the bandwidth enhancement, thus covering the frequency band 24.5-26.6 GHz, as exhibited in Figure. 4 (c).

The design is further progressed to obtain MIMO capability. The four antenna elements are placed along the opposite edges, with a substrate size of 30 mm × 43 mm × 0.787 mm, as illustrated in Figure. 4 (b). In addition, the ground plane has defected with horizontal slots exactly beneath the four MIMO antennas. The simulated reflection coefficient results plotted in Figure. 4 (c) for the MIMO antennas (S_{11}, S_{22}, S_{33}, and S_{44}) exhibit nearly similar behavior, resonating for the band ranging from 24.8-26.15 GHz. This demonstrates that the bandwidth obtained by the MIMO antennas is narrow as compared to the two-element array. This insignificant degradation in bandwidth is mainly due to the near field coupling effects. Despite the fact that bandwidth has narrowed for the MIMO structure, the attained bandwidth is sufficient enough to enable the mm-Wave operation. Figure. 4 (d) depicts the

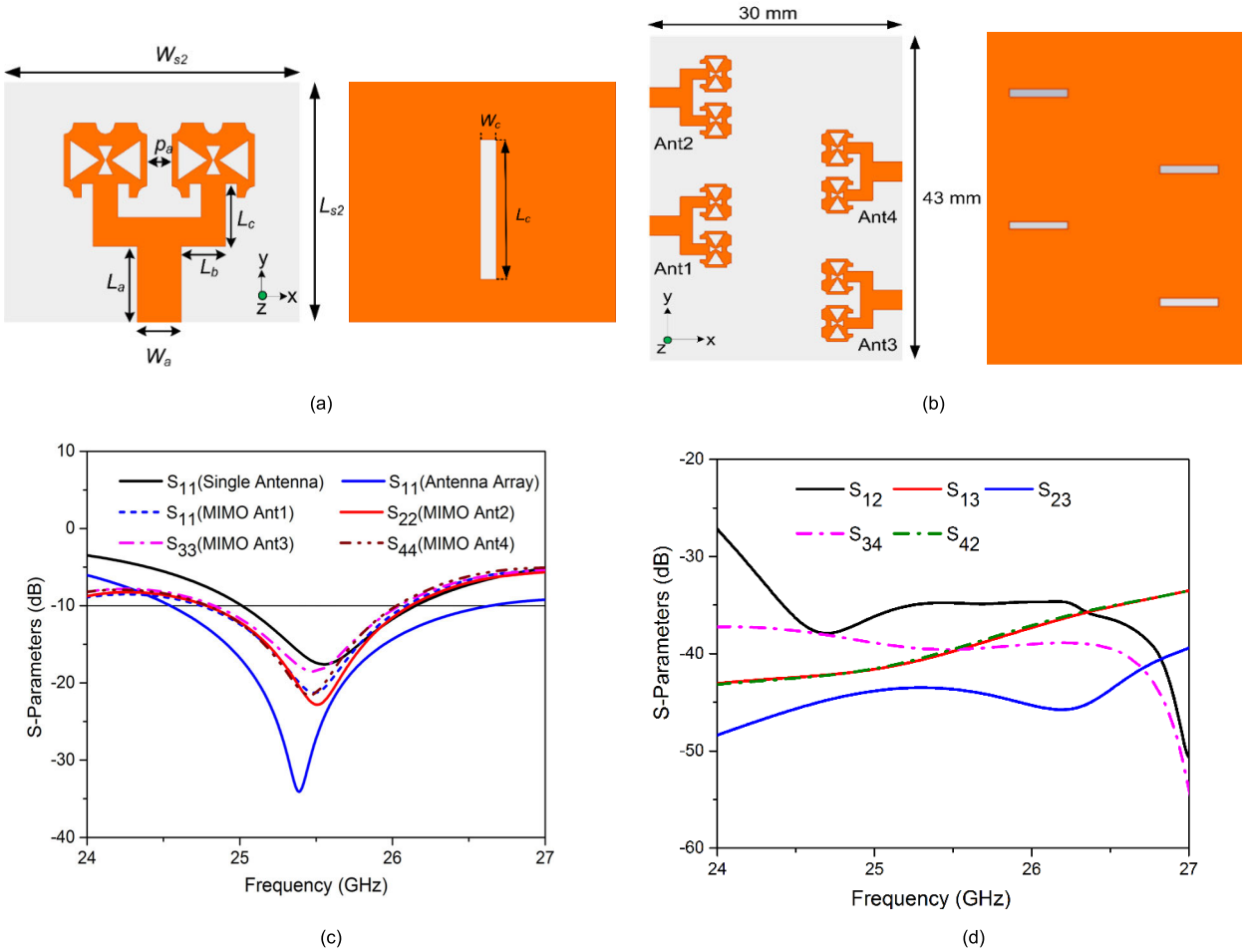

FIGURE 4. (a) Top and bottom view of antenna array (b) Layout of MIMO antenna (c) Reflection coefficient (d) Transmission coefficient.

transmission coefficient plots, where significant isolation has been obtained for different MIMO antennas, where the minimum value near −33 dB is obtained between Ant1 and Ant2 over the entire operating frequency band.

B. METASURFACE ARRAY DESIGN

The reflection coefficient results of the MIMO antennas exhibit degradation in the antenna characteristics primarily due to coupling effects. In order to enhance the radiation performance of the antenna in terms of operating bandwidth, antenna gain, and isolation between MIMO elements, an eminent technique is to employ metasurface. A metasurface is basically a periodical placement of unit cells at a specific distance from each other.

The unit cell in this work is designed at 26 GHz. The substrate used is Rogers RT Duriod 5880 with 0.787 mm thickness. CST in the time domain is used to perform the simulations of a unit cell. The final optimized unit cell consists of two circular split ring resonators with a circular geometrical pattern in the centre, as illustrated in Figure. 5 (a). Figure. 5 (a) also depicts the step wise evolution of the unit cell. Figure 5 (b) illustrates the boundary conditions and the ports assignment to excite the unit cell. The reflection coefficient curve of the unit cell in Figure. 5(c) clearly exhibits unit cell is resonating at 26 GHz. Also the transmission coefficient plot shows that the unit cell loss is nearly zero at the resonating frequency, thus ascertains the full transmission at the desired band.

In order to further elaborate the behavior of metamaterial unit cell, the integral parameters such as permittivity (ε) and permeability (μ) are also investigated by applying the technique as provided in [44]. For permittivity and permeability extraction, equations (8-11) are used.

$$z = \pm \sqrt{\frac{(1 + S_{ii})^2 - S_{ji}^2}{(1 - S_{ii})^2 - S_{ji}^2}} \tag{8}$$

$$e^{j\eta k_o d} = \frac{S_{ji}}{1 - S_{ii}\frac{z-1}{z+1}} \tag{9}$$

where S_{ii} is the reflection coefficient, S_{ji} is transmission coefficient, k_o is the wavenumber, z is the normalized impedance, d is the thickness of the material, and η is the refractive index.

$$\varepsilon = \frac{\eta}{z} \tag{10}$$

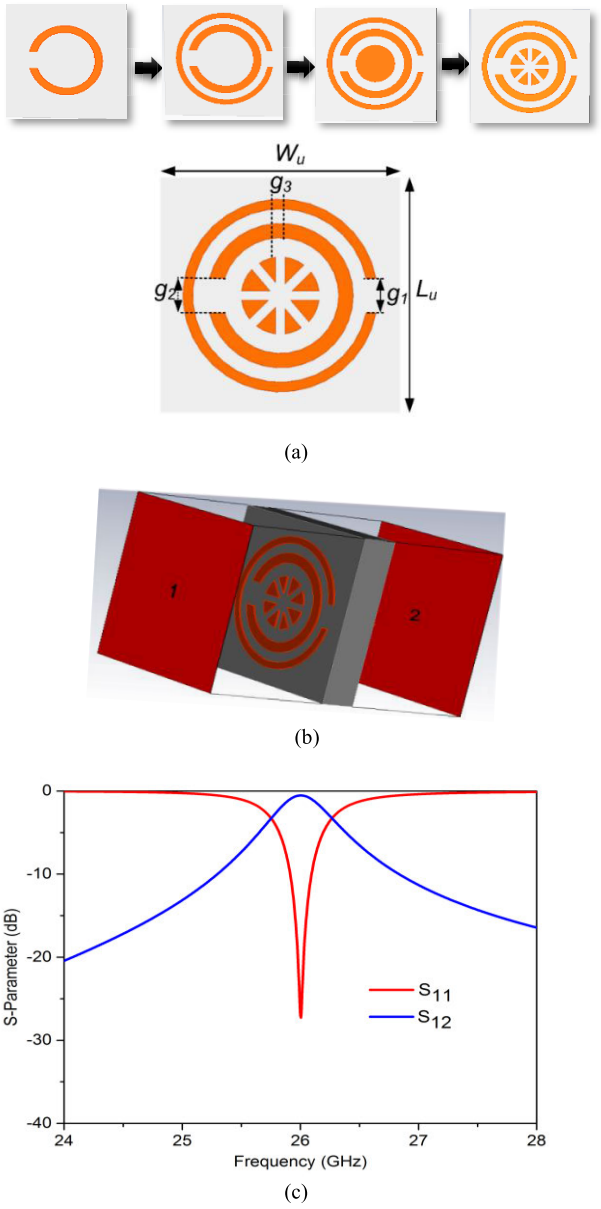

FIGURE 5. (a) Unit cell design (b) Unit cell excitation (c) S-parameter curves of unit cell.

$$\mu = \eta \times z \tag{11}$$

where ε is the relative permittivity, while μ is the relative permeability. Figure. 6 depicts the permittivity and permeability plots of the unit cell. It is observed that both permittivity and permeability tend to zero at the 26 GHz, which demonstrates zero refractive indexes [45].

Later, a metasurface array is obtained by periodically placing 9 × 6 unit cells at a spacing of g, as Figure. 7 (a) illustrates. The dimensions of the metasurface are $W_m \times L_m$. The metasurface is stacked above the MIMO antennas, as illustrated in Figure. 7 (b), at a distance of h_t to enhance the antenna performance. After incorporation of metasurface, the MIMO antennas show significant improvement in

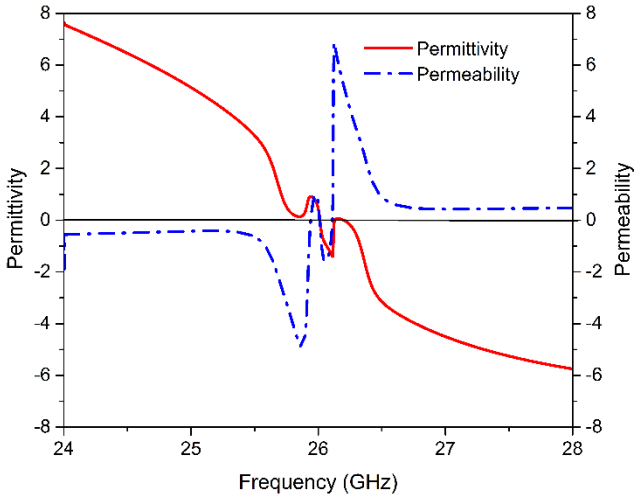

FIGURE 6. Extracted parameters of the Unit cell.

performance, as exhibited in Figure. 8 (a) and (b). The reflection coefficient plots of MIMO antennas before and after metasurface employment in Figure. 8 (a) depicts the improvement in impedance bandwidth from 1.35 GHz to 1.92 GHz, thus covering the frequency band 24.48-26.4 GHz. As other antennas exhibit the nearly same behavior, therefore the curves for only Ant1 and Ant4 are shown here. While the transmission coefficients curve in Figure. 8 (b) depicts the minimum isolation among Ant1 and Ant2 with metasurface, which is approximately −38 dB. At the same time, the Ant1 and Ant3 exhibit minimum isolation of −40 dB over the entire operational frequency band. The same behavior is observed for Ant2 and Ant4. The maximum isolation is achieved for Ant2 and Ant3 approaching a value of −45 dB. These transmission coefficient curves clearly provides evidence that minimum isolation is improved by 5dB after metasurface employment.

In order to further elaborate on the contribution of metasurface in isolation enhancement by repressing the surface waves [33], surface current distribution is investigated at 26 GHz. The surface current distribution is shown in Figure. 9 exhibits that the near-field coupling effect is cancelled as the current coupled to unit cell traverses in the opposite direction in half of the ring as well as in adjacent rings. It is also observed that without metasurface when Ant1 is excited while other antennas are terminated with 50Ω load, the current is mainly coupled to Ant2, whereas lower coupling is noticed for Ant3 and Ant4. With metasurface placed above, the coupled field between antenna elements is primarily distributed on the unit cells of the metasurface. Consequently, coupling between antenna elements is minimized and, the isolation is improved significantly.

Similarly, Figure. 10 provides a comparative analysis of the simulated broadside gain of antenna for different steps of design evolution at various frequencies of the operating band. It is observed that the gain of the antenna is increased

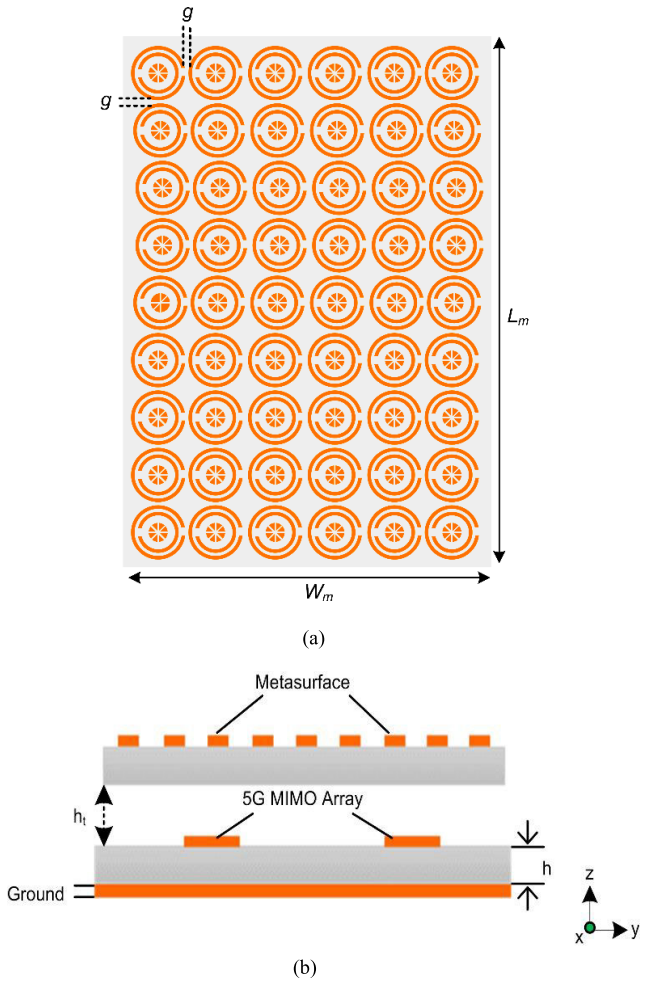

FIGURE 7. (a) 9 × 6 metasurface array (b) Side view of antenna with metasurface on top.

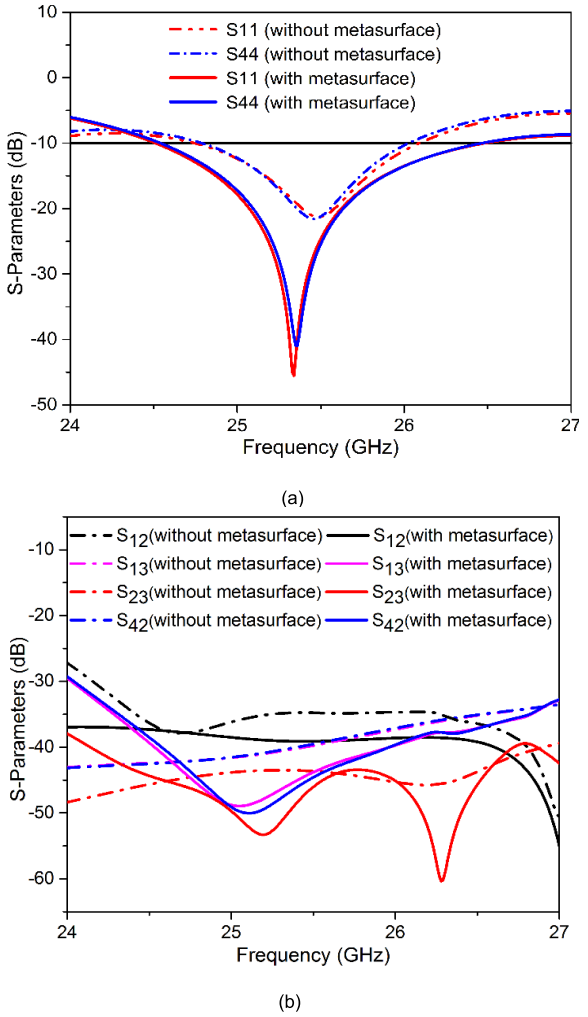

FIGURE 8. S-parameter results without and with metasurface (a) Reflection coefficient (b) Transmission coefficient.

at the first step by modifying the single element antenna to a two element array structure, from 6.8 dBi to 8.1 dBi at 26 GHz. The antenna gain for the MIMO configuration nearly remains the same, however after employing metasurface, gain increases by approximately 2.2 dBi. Here the metasurface acts as a superstrate layer, which generates a resonant cavity effect resulting in gain enhancement of the antenna system [46], [47]. Thus, the peak simulated gain obtained is 10.37 dBi for Ant1 and 10.15 dBi for Ant4 at 26 GHz.

III. EXPERIMENTAL RESULTS

The proposed MIMO antenna with metasurface is fabricated, as shown in Figure. 11 (a), for experimental validation. In order to stack the metasurface above the antennas, Nylon spacers are used. The comparative investigation of simulated and measured results is provided in the succeeding sections.

A. REFLECTION COEFFICIENT AND ISOLATION

For S-parameters measurement, the Rohde and Schwarz ZVA 40 Vector Network Analyzer (VNA) is used. Simulated

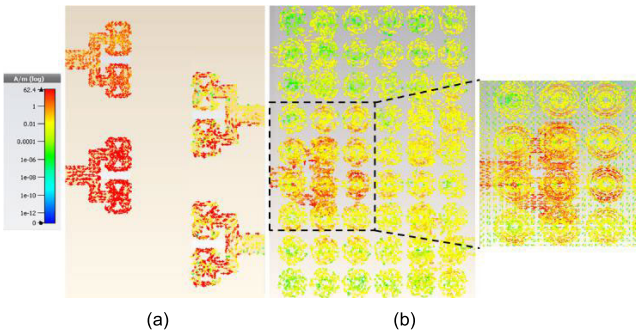

FIGURE 9. Surface current distribution at 26 GHz (a) Without metasurface (b) with metasurface.

and measured S-parameter results are demonstrated in Figure. 12 (a), (b). The measured reflection coefficient results for Ant1 and Ant4 are illustrated in Figure. 12 (a) demonstrates that Ant1 resonates for the 24.7-26.4 GHz frequency band with −10 dB impedance bandwidth of 1.7 GHz. Similarly, the operational frequency band for Ant4 ranges

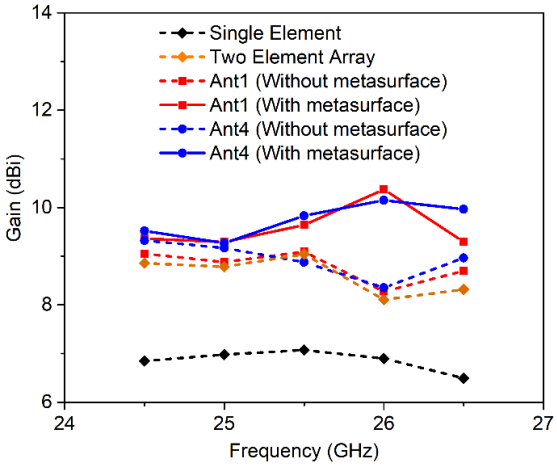

FIGURE 10. Simulated broadside gain of MIMO antennas.

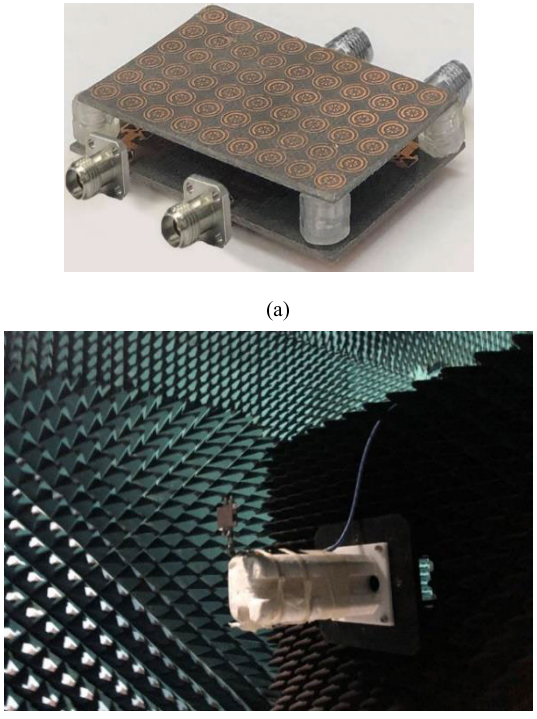

FIGURE 11. (a) Fabricated antenna (b) Far-field measurement setup.

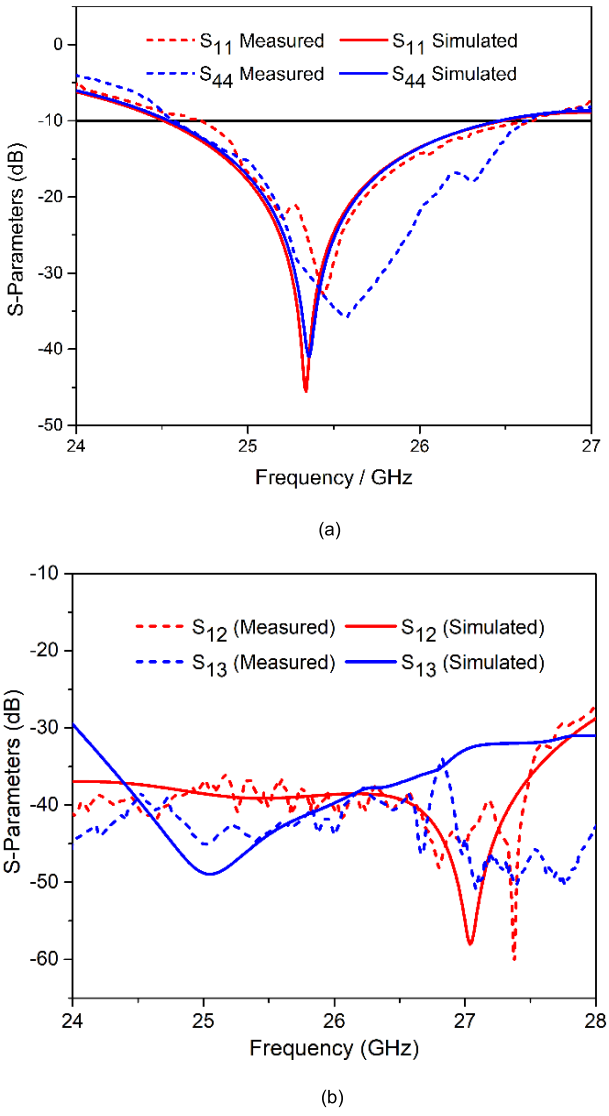

FIGURE 12. Measured and simulated S-parameter results (a) Reflection coefficient (b) Transmission coefficient.

from 24.55-26.5 GHz with an impedance bandwidth of 1.95 GHz. Moreover, Figure 12 (b) shows the measured transmission coefficient curves demonstrating isolation of Ant1 with Ant2 and Ant3. It is observed that measured and simulated results have minimal discontinuities, mainly due to flaws in fabrication and losses across the cable.

B. RADIATION PATTERN AND GAIN

The far-field results of the antenna are obtained in the anechoic chamber at the Electromagnetic Wave Technology Institute, Seoul, Korea. A standard gain horn antenna (SGH-series) is used as a transmitter (TX), while the proposed antenna is measured as a receiver (RX). In order to provide stable power reception, amplifiers were used. The antenna under test is rotated to obtain measurements at different orientations. The radiation patterns in the XZ and YZ plane for Ant1 and Ant4 at 26 GHz are shown in Figure 13 (a) and (b). It is observed that in the XZ plane, Ant1 exhibits maximum radiation at $\theta = 25°$, whereas Ant4 demonstrates the main beam in the direction of $\theta = -16°$.

The measured and simulated antenna gain values of the proposed antenna with metasurface at different frequencies are tabulated in Table 2. It is demonstrated that the Ant1 attained the measured peak gain of 10.21 dBi at 26 GHz. Whereas, for Ant4, the maximum value of gain measured is

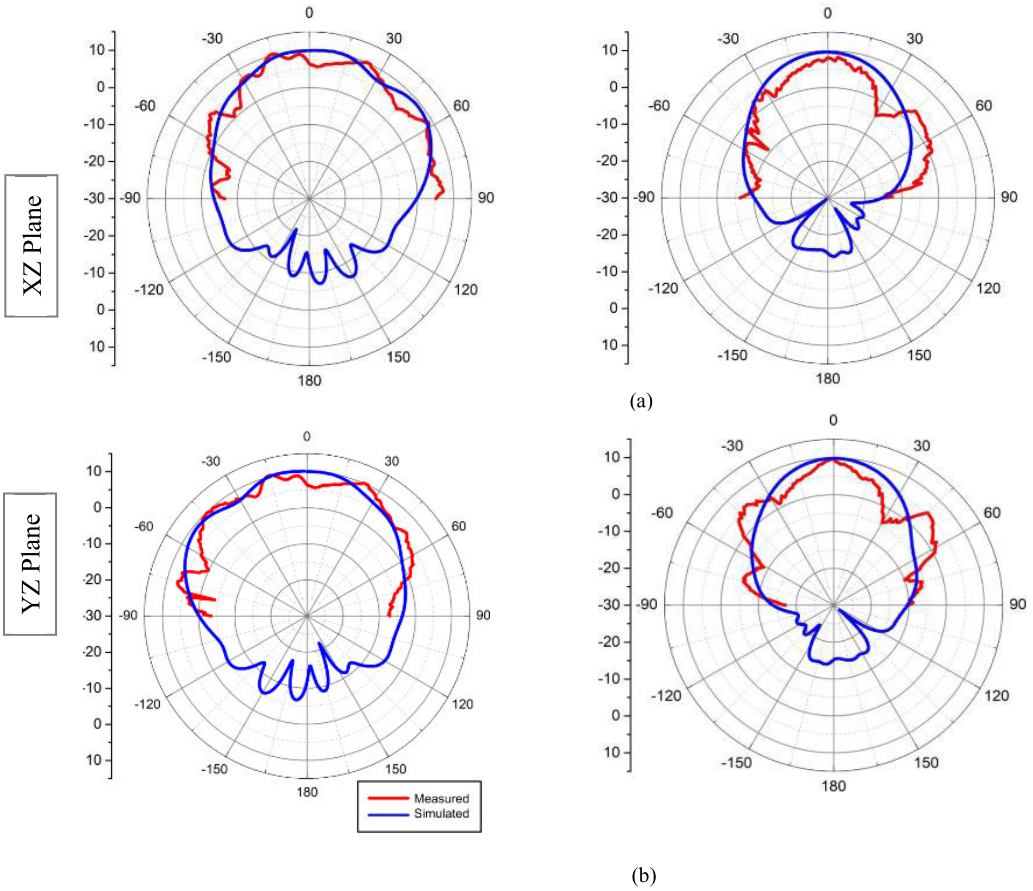

FIGURE 13. Radiation patterns at 26 GHz (a) Ant 1 (b) Ant4.

TABLE 2. Gain of proposed MIMO antennas.

Frequency (GHz)	Ant#	Peak Gain (dBi)	
		Simulated	Measured
24.5	Ant1	9.35	9.31
	Ant4	9.52	9.56
25.5	Ant1	9.64	9.47
	Ant4	9.83	9.91
26	Ant1	10.37	10.21
	Ant4	10.15	10.27

10.27 dBi. Thus, coherence is observed amid the measured and simulated results.

IV. MIMO PERFORMANCE

In order to analyze the MIMO performance of an antenna, different parameters, including ECC, DG, MEG, and CCL, are of great significance. For the proposed antenna design, these parameters are discussed in the following subsections.

A. ECC AND DG

ECC for any MIMO system determines the correlation between the individual elements in terms of their individual characteristics. For ECC calculation, equation (12) is used as given in [48], [49].

$$\rho_{ec,ij} = \frac{\left|S_{ii} * S_{ij} + S_{ji} * S_{jj}\right|^2}{\left(1 - |S_{ii}|^2 - S_{ij}^2\right)\left(1 - \left|S_{ji}\right|^2 - S_{jj}^2\right)} \tag{12}$$

where S_{ii} is the reflection coefficient of antenna i while S_{ij} (where $i \neq j$) is the transmission coefficient for antennas i and j. The ECC plot for the proposed design is illustrated in Figure. 14 clearly shows that the obtained values are far below the practically acceptable value, which is 0.5 for wireless systems.

Similarly, diversity gain is another substantial MIMO performance metric. It demonstrates the extent of transmission power reduction after using a diversity scheme. Diversity gain is obtained using the relation (13), as provided in [50].

$$D_{iG} = 10\sqrt{1 - \left|\rho_{ec,ij}\right|^2} \tag{13}$$

Figure. 14 also depicts the plots of diversity gain. Diversity gain of approximately 9.98 dB is attained for Ant1 & Ant3,

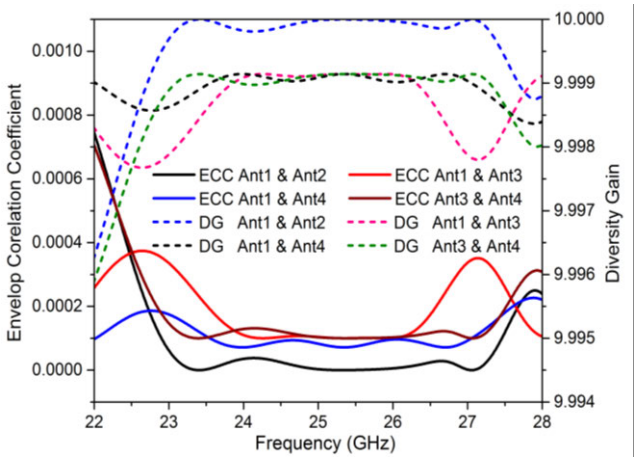

FIGURE 14. ECC and DG of MIMO antennas.

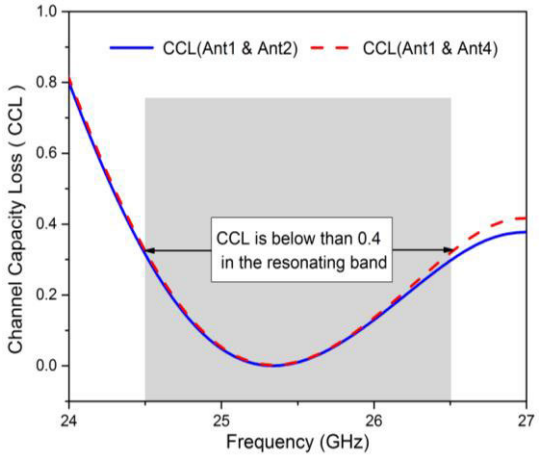

FIGURE 15. Channel capacity loss of proposed MIMO antenna.

TABLE 3. Mean effective gain of proposed MIMO antenna.

Frequency (GHz)	Ant1 (-dB)	Ant2 (-dB)	Ant3 (-dB)	Ant4 (-dB)
24.5	6.402	6.403	6.449	6.443
25	6.170	6.167	6.194	6.192
25.5	6.059	6.051	6.046	6.054
26	6.432	6.403	6.400	6.429
26.5	6.971	6.877	6.907	6.993

Ant1 & Ant4, and Ant3 & Ant4, whereas for Ant1 & Ant2 the obtained value of DG is 9.999 dB.

B. MEG

Mean Effective Gain also has significance in analyzing the performance of MIMO antennas, which is actually the ratio of mean received power to the mean incident power. Equation (14) is used to estimate the value of MEG as given in [32].

$$ME_fG = 1/2(1 - \sum_{j=1}^{k} S_{ij}) \tag{14}$$

The standard value of the Mean effective gain (ME_fG) for good diversity performance should be

$$-3\ dB \leq ME_fG \leq -12dB$$

The numerical values of MEG obtained for the proposed MIMO antennas are given in Table 3.

C. CHANNEL CAPACITY LOSS (CLL)

In general, with the increase in a number of antenna elements in the MIMO system, the channel capacity also increases. CCL determines the channel's capacity loss due to the correlation between the MIMO links. CCL can be calculated using the equations (15)-(18) as given in [32].

$$C\ (loss) = -log_2 det\ (a_k) \tag{15}$$

where a_k is correlation Matrix.

$$a_k = \begin{bmatrix} \sigma_{11} & \sigma_{12} \\ \sigma_{21} & \sigma_{22} \end{bmatrix} \tag{16}$$

where,

$$\sigma_{ii} = 1 - \left(|S_{ii}|^2 - |S_{jj}|^2\right) \tag{17}$$

$$\sigma_{ij} = -\left(S_{ii} * S_{ij} + S_{ji}S_{jj}^*\right) \tag{18}$$

where σ_{ii} and σ_{ij} are the correlation coefficients between the antenna elements ii and ij of MIMO antenna. CCL for the proposed MIMO design is depicted in Figure. 15. It is clearly shown that CCL is below the practically acceptable value of 0.4 bit/s/Hz over the operating band. Thus the high throughput of the proposed system is ascertained.

V. COMPARISON WITH THE RELATED WORK

The proposed 5G mm-Wave MIMO antenna with metasurface array is compared with the recently reported literary works, as shown in Table 4. It is observed that the proposed MIMO antenna with metasurface array outperforms the other reported works in terms of isolation. Moreover, the antenna gain exhibited by proposed MIMO antenna is significantly higher than the works [32], [34], [36], [38]–[40]. Although the works presented in [35], [37] achieved higher gain as compared to the proposed antenna, however, these MIMO structures have only two elements, and also MIMO performance analysis is not provided. The presented antenna design demonstrates improved MIMO performance in comparison to other antennas discussed here. Consequently, the pertinence of the proposed MIMO antenna is ascertained for current and future communication devices.

TABLE 4. Comparison with related work.

Ref	No. of ports	Optimization Techniques	f_c (GHz)	Gain (dBi)	Isolation (dB)	ECC (dB)	CCL (Bits/sec/Hz)
[32]	4	MIMO +DGS	28	8.3	-17	<0.5	<0.4
[34]	4	MIMO +FSS	30	Not provided	-25	Not calculated	Not Calculated
[35]	2	MIMO + Metasurface	28	16-17	-37	Not calculated	Not calculated
[36]	2	MIMO + Metamaterial based PR wall	60	Not provided	-22	$<0.1e^{-6}$	Not calculated
[37]	2	MIMO+EBG	28, 38	11.5, 10.9	-20	<0.12	Not calculated
[38]	1	Metamaterial array	26	7.4	N/A	N/A	N/A
[39]	2	MIMO+ EBG	24	6	-37	≅0.24	Not calculated
[40]	4	DRA-based MIMO+ Metamaterial	28	7	-29.34	0.02	Not calculated
This work	4	MIMO + Metasurface	26	10.27	-45	$<0.1\ e^{-6}$	<0.4

VI. CONCLUSION

A four element MIMO antenna using single-layered metasurface is presented, supporting mm-Wave 5G applications. Each MIMO element is composed of a 1×2 antenna array with a parallel feeding network. While, the metasurface comprises of 9×6 unit cell array, where each unit cell is a Circular Split Ring (CSR) shaped resonator. The MIMO antenna covers the 26 GHz band with measured impedance bandwidth of 1.95 GHz. Moreover, the placement of metasurface above the MIMO antennas at a distance of approx. 0.5λ not only enhance the isolation between the antenna elements but also improves the gain by 2.1 dBi with a peak measured gain of 10.27 dBi. In addition, the MIMO performance analysis demonstrated good diversity performance with low correlation coefficients and channel capacity loss. This validates that the proposed MIMO antenna is appropriate for 5G mm-Wave communication systems.

REFERENCES

[1] Qualcomm Technologies. (Dec. 2017). *Spectrum for 4G and 5G*. Accessed: Jan. 5, 2019. [Online]. Available: https://www.qualcomm.com/news/media-center

[2] J. Thompson, X. Ge, H.-C. Wu, R. Irmer, H. Jiang, G. Fettweis, and S. Alamouti, "5G wireless communication systems: Prospects and challenges [guest editorial]," *IEEE Commun. Mag.*, vol. 52, no. 2, pp. 62–64, Feb. 2014.

[3] C.-X. Wang, F. Haider, X. Gao, X.-H. You, Y. Yang, D. Yuan, H. Aggoune, H. Haas, S. Fletcher, and E. Hepsaydir, "Cellular architecture and key technologies for 5G wireless communication networks," *IEEE Commun. Mag.*, vol. 52, no. 2, pp. 122–130, Feb. 2014.

[4] L. Wei, R. Q. Hu, Y. Qian, and G. Wu, "Key elements to enable millimeter wave communications for 5G wireless systems," *IEEE Wireless Commun.*, vol. 21, no. 6, pp. 136–143, Dec. 2014.

[5] S. Rangan, T. S. Rappaport, and E. Erkip, "Millimeter-wave cellular wireless networks: Potentials and challenges," *Proc. IEEE*, vol. 102, no. 3, pp. 366–385, Mar. 2014.

[6] T. S. Rappaport, S. Sun, R. Mayzus, H. Zhao, Y. Azar, K. Wang, G. N. Wong, J. K. Schulz, M. Samimi, and F. Gutierrez, "Millimeter wave mobile communications for 5G cellular: It will work!" *IEEE Access*, vol. 1, pp. 335–349, 2013.

[7] European 5G Observatory. *National 5G Spectrum Assignment*. Accessed: May 10, 2020. [Online]. Available: https://5gobservatory.eu/

[8] B. Biglarbegian, M. Fakharzadeh, D. Busuioc, M.-R. Nezhad-Ahmadi, and S. Safavi-Naeini, "Optimized microstrip antenna arrays for emerging millimeter-wave wireless applications," *IEEE Trans. Antennas Propag.*, vol. 59, no. 5, pp. 1742–1747, May 2011.

[9] Y. Li and K. M. Luk, "Wideband perforated dense dielectric patch antenna array for millimeter-wave applications," *IEEE Trans. Antennas Propag.*, vol. 63, no. 8, pp. 3780–3786, Aug. 2015.

[10] S. X. Ta, H. Choo, and I. Park, "Broadband printed-dipole antenna and its arrays for 5G applications," *IEEE Antennas Wireless Propag. Lett.*, vol. 16, pp. 2183–2186, 2017.

[11] Z. Briqech, A.-R. Sebak, and T. A. Denidni, "Low-cost wideband mm-wave phased array using the piezoelectric transducer for 5G applications," *IEEE Trans. Antennas Propag.*, vol. 65, no. 12, pp. 6403–6412, Dec. 2017.

[12] P. A. Dzagbletey and Y.-B. Jung, "Stacked microstrip linear array for millimeter-wave 5G baseband communication," *IEEE Antennas Wireless Propag. Lett.*, vol. 17, no. 5, pp. 780–783, May 2018.

[13] M. Khalily, R. Tafazolli, P. Xiao, and A. A. Kishk, "Broadband mm-wave microstrip array antenna with improved radiation characteristics for different 5G applications," *IEEE Trans. Antennas Propag.*, vol. 66, no. 9, pp. 4641–4647, Sep. 2018.

[14] S. Zhu, H. Liu, Z. Chen, and P. Wen, "A compact gain-enhanced Vivaldi antenna array with suppressed mutual coupling for 5G mmWave application," *IEEE Antennas Wireless Propag. Lett.*, vol. 17, no. 5, pp. 776–779, Mar. 2018.

[15] S. I. Naqvi, A. H. Naqvi, F. Arshad, M. A. Riaz, M. A. Azam, M. S. Khan, Y. Amin, J. Loo, and H. Tenhunen, "An integrated antenna system for 4G and millimeter-wave 5G future handheld devices," *IEEE Access*, vol. 7, pp. 116555–116566, 2019.
[16] B. Yu, K. Yang, C.-Y.-D. Sim, and G. Yang, "A novel 28 GHz beam steering array for 5G mobile device with metallic casing application," *IEEE Trans. Antennas Propag.*, vol. 66, no. 1, pp. 462–466, Jan. 2018.
[17] J. Bang and J. Choi, "A SAR reduced mm-wave beam-steerable array antenna with dual-mode operation for fully metal-covered 5G cellular handsets," *IEEE Antennas Wireless Propag. Lett.*, vol. 17, no. 6, pp. 1118–1122, Jun. 2018.
[18] M. J. Al-Hasan, T. A. Denidni, and A. R. Sebak, "Millimeter-wave EBG-based aperture-coupled dielectric resonator antenna," *IEEE Trans. Antennas Propag.*, vol. 61, no. 8, pp. 4354–4357, Aug. 2013.
[19] O. M. Haraz, A. Elboushi, S. A. Alshebeili, and A.-R. Sebak, "Dense dielectric patch array antenna with improved radiation characteristics using EBG ground structure and dielectric superstrate for future 5G cellular networks," *IEEE Access*, vol. 2, pp. 909–913, 2014.
[20] M. Akbari, S. Gupta, M. Farahani, A. R. Sebak, and T. A. Denidni, "Gain enhancement of circularly polarized dielectric resonator antenna based on FSS superstrate for MMW applications," *IEEE Trans. Antennas Propag.*, vol. 64, no. 12, pp. 5542–5546, Dec. 2016.
[21] L. Mall and R. B. Waterhouse, "Millimeter-wave proximity-coupled microstrip antenna on an extended hemispherical dielectric lens," *IEEE Trans. Antennas Propag.*, vol. 49, no. 12, pp. 1769–1772, Dec. 2001.
[22] B. T. Malik, V. Doychinov, S. A. R. Zaidi, I. D. Robertson, and N. Somjit, "Antenna gain enhancement by using low-infill 3D-printed dielectric lens antennas," *IEEE Access*, vol. 7, pp. 102467–102476, 2019.
[23] H. Attia, M. L. Abdelghani, and T. A. Denidni, "Wideband and high-gain millimeter-wave antenna based on FSS Fabry–Pérot cavity," *IEEE Trans. Antennas Propag.*, vol. 65, no. 10, pp. 5589–5594, Oct. 2017.
[24] N. Hussain and I. Park, "Performance of multiple feed metasurface antennas with different numbers of patch cells and different substrate thicknesses," *Appl. Comput. Electromagn. J.*, vol. 33, no. 1, pp. 49–55, 2018.
[25] M. Asaadi, I. Afifi, and A.-R. Sebak, "High gain and wideband high dense dielectric patch antenna using FSS superstrate for millimeter-wave applications," *IEEE Access*, vol. 6, pp. 38243–38250, 2018.
[26] S. F. Jilani and A. Alomainy, "Millimetre-wave T-shaped MIMO antenna with defected ground structures for 5G cellular networks," *IET Microw., Antennas Propag.*, vol. 12, no. 5, pp. 672–677, Apr. 2018.
[27] N. Shoaib, S. Shoaib, R. Y. Khattak, I. Shoaib, X. Chen, and A. Perwaiz, "MIMO antennas for smart 5G devices," *IEEE Access*, vol. 6, pp. 77014–77021, 2018.
[28] F. Wang, Z. Duan, X. Wang, Q. Zhou, and Y. Gong, "High isolation millimeter-wave wideband MIMO antenna for 5G communication," *Int. J. Antennas Propag.*, vol. 2019, pp. 1–12, May 2019.
[29] M. S. Sharawi, S. K. Podilchak, M. T. Hussain, and Y. M. M. Antar, "Dielectric resonator based MIMO antenna system enabling millimetre-wave mobile devices," *IET Microw., Antennas Propag.*, vol. 11, no. 2, pp. 287–293, Jan. 2017.
[30] Y. M. Pan, X. Qin, Y. X. Sun, and S. Y. Zheng, "A simple decoupling method for 5G millimeter-wave MIMO dielectric resonator antennas," *IEEE Trans. Antennas Propag.*, vol. 67, no. 4, pp. 2224–2234, Apr. 2019.
[31] W. Ali, S. Das, H. Medkour, and S. Lakrit, "Planar dual-band 27/39 GHz millimeter-wave MIMO antenna for 5G applications," *Microsyst. Technol.*, vol. 27, pp. 1–10, Jan. 2020.
[32] M. Khalid, S. I. Naqvi, N. Hussain, M. Rahman, Fawad, S. S. Mirjavadi, M. J. Khan, and Y. Amin, "4-port MIMO antenna with defected ground structure for 5G millimeter wave applications," *Electronics*, vol. 9, no. 1, p. 71, Jan. 2020.
[33] A. Li, S. Singh, and D. Sievenpiper, "Metasurfaces and their applications," *Nanophotonics*, vol. 7, no. 6, pp. 989–1011, 2018.
[34] M. Akbari, H. A. Ghalyon, M. Farahani, A.-R. Sebak, and T. A. Denidni, "Spatially decoupling of CP antennas based on FSS for 30-GHz MIMO systems," *IEEE Access*, vol. 5, pp. 6527–6537, 2017.
[35] S. Gupta, Z. Briqech, A. R. Sebak, and T. A. Denidni, "Mutual-coupling reduction using metasurface corrugations for 28 GHz MIMO applications," *IEEE Antennas Wireless Propag. Lett.*, vol. 16, pp. 2763–2766, 2017.
[36] M. Farahani, J. Pourahmadazar, M. Akbari, M. Nedil, A. R. Sebak, and T. A. Denidni, "Mutual coupling reduction in millimeter-wave MIMO antenna array using a metamaterial polarization-rotator wall," *IEEE Antennas Wireless Propag. Lett.*, vol. 16, pp. 2324–2327, 2017.
[37] A. A. R. Saad and H. A. Mohamed, "Printed millimeter-wave MIMO-based slot antenna arrays for 5G networks," *AEU Int. J. Electron. Commun.*, vol. 99, pp. 59–69, Feb. 2019.
[38] H. Jiang, L.-M. Si, W. Hu, and X. Lv, "A symmetrical dual-beam bowtie antenna with gain enhancement using metamaterial for 5G MIMO applications," *IEEE Photon. J.*, vol. 11, no. 1, pp. 1–9, Feb. 2019.
[39] A. Iqbal, A. Basir, A. Smida, N. K. Mallat, I. Elfergani, J. Rodriguez, and S. Kim, "Electromagnetic bandgap backed millimeter-wave MIMO antenna for wearable applications," *IEEE Access*, vol. 7, pp. 111135–111144, 2019.
[40] N. S. Murthy, "Improved isolation metamaterial inspired mm-Wave MIMO dielectric resonator antenna for 5G application," *Prog. Electromagn. Res. C*, vol. 100, pp. 247–261, Mar. 2020.
[41] C. A. Balanis, *Antenna Theory: Analysis and Design*, 3rd ed. Hoboken, NJ, USA: Wiley, 2005.
[42] O. Yurduseven, D. Smith, and M. Elsdon, "Printed slot loaded bow-tie antenna with super wideband radiation characteristics for imaging applications," *IEEE Trans. Antennas Propag.*, vol. 61, no. 12, pp. 6206–6210, Dec. 2013.
[43] M. R. Islam, "Study and implementation of wideband bow-tie antennas," M.S. thesis, Georgia Southern Univ., Statesboro, GA, USA, 2017.
[44] D. R. Smith, S. Schultz, P. Markoš, and C. M. Soukoulis, "Determination of effective permittivity and permeability of metamaterials from reflection and transmission coefficients," *Phys. Rev. B, Condens. Matter*, vol. 65, no. 19, Apr. 2002, Art. no. 195104.
[45] P. K. Panda and D. Ghosh, "Isolation and gain enhancement of patch antennas using EMNZ superstrate," *AEU Int. J. Electron. Commun.*, vol. 86, pp. 164–170, Mar. 2018.
[46] T. J. Cui, D. Smith, and R. Liu, *Metamaterials: Theory, Design, and Applications*. New York, NY, USA: Springer, 2009.
[47] N. Hussain, M.-J. Jeong, J. Park, and N. Kim, "A broadband circularly polarized Fabry–Perot resonant antenna using a single-layered PRS for 5G MIMO applications," *IEEE Access*, vol. 7, pp. 42897–42907, 2019.
[48] S. Blanch, J. Romeu, and I. Corbella, "Exact representation of antenna system diversity performance from input parameter description," *Electron. Lett.*, vol. 39, no. 9, pp. 705–707, May 2003.
[49] M. S. Sharawi, "Printed multi-band MIMO antenna systems and their performance metrics [wireless corner]," *IEEE Antennas Propag. Mag.*, vol. 55, no. 5, pp. 218–232, Oct. 2013.
[50] M. S. Sharawi, *Printed MIMO Antenna Engineering*. Norwood, MA, USA: Artech House, 2014.

SABA TARIQ received the bachelor's degree in telecommunication engineering from the University of Engineering and Technology, Taxila, Pakistan, in 2018. She is currently pursuing the master's degree. Her research interests include the antenna array designs and MIMO antenna designs for millimeter wave 5G applications.

SYEDA I. NAQVI received the B.Sc. Engineering degree in computer engineering and the M.Sc. degree in telecommunication engineering from the University of Engineering and Technology, Taxila, Pakistan, in 2006 and 2011, respectively. She is currently serving as an Assistant Professor with the University of Engineering and Technology. She is working towards the design and implementation of multiple antenna array systems for current 4G and next generation millimeter-wave 5G applications.

NIAMAT HUSSAIN (Member, IEEE) received the B.S. degree in electronics engineering from the Dawood University of Engineering and Technology, Karachi, Pakistan, in 2014, the M.S. degree in electrical and computer engineering from Ajou University, Suwon, South Korea, and the Ph.D. degree in information and communication engineering from Chungbuk National University, Chungju-si, South Korea. He is currently a Postdoctoral Researcher with Chungbuk National University. His research interests include lens-coupled antennas, metasurface antennas, metamaterial antennas, UWB antennas, mmWave antennas, and terahertz antennas. He has received Best Paper Award, in 2017, for his presented paper at Korea Winter Conference (KIEES).

YASAR AMIN (Senior Member, IEEE) received the B.Sc. degree in electrical engineering with a focus on telecommunication and the M.B.A. degree in innovation and growth from the Turku School of Economics, University of Turku, Finland, and the M.Sc. degree in electrical engineering with a focus on system on chip design and the Ph.D. degree in electronic and computer systems from the KTH Royal Institute of Technology, Sweden, with the research focus on printable green RFID antennas for embedded sensors. He is currently a Professor and the Chairman of the Department of Telecommunication Engineering, University of Engineering and Technology Taxila, Pakistan. He also serves as the Director of Embedded Systems Research and Development Centre. He is the founder of Agile Creative Technologies for Smart Electromagnetic Novel Applications (ACTSENA) Research Group. He has authored or coauthored more than 100 international technical papers in conferences and journals. His research interests include the design and application of multiple antenna systems for next generation mobile communication systems, millimeter-wave and terahertz antenna array, implantable and wearable electronics, and inkjet printing technology in microwave applications. He is a member of more than a dozen international professional societies and the Fellow of PAE.